COMPRESSED SENSING RECONSTRUCTION OF STATISTICAL PARAMETER MAP FOR FUNCTIONAL DIFFUSE OPTICAL TOMOGRAPHY

Ok Kyun Lee[1]*, Hua Li*[1]*, Sung Ho Tak*[1] *and Jong Chul Ye*[1]

[1] Dept. of Bio and Brain Engineering, KAIST
291 Daehak-ro Yuseong-gu, Daejon 305-701, Republic of Korea

ABSTRACT

Functional near infrared spectroscopy (fNIRS) is a non-invasive imaging modality to measure functional brain activities. Many researches have investigated diffuse optical tomography (DOT) to overcome the limitation of lack of depth information in fNIRS topographic approach. In this paper, we proposes a novel compressed sensing approach, especially using a 2-thresholding algorithm, that directly reconstructs statistical parameter maps by exploiting spatio-temporal sparsity of neural activation. The final reconstruction algorithm has very intuitive form which is similar to conventional fDOT with SPM analysis. However, the main advantage of the new algorithm is that the unknown weighting components in inversion kernel are iteratively updated for more accurate reconstruction which significantly improves the reconstruction performance. Experimental results demonstrated that the localization error using the proposed method is competitive with that of fMRI.

Index Terms— Diffuse optical tomography, compressed sensing, 2-thresholding, general linear model, spatio-temporal constraint, statistical parametric mapping

1. INTRODUCTION

Since optical absorption is related to the changes of cerebral blood volume (CBV) and cerebral blood oxygenation, NIRS can image brain metabolism via monitoring total hemoglobin (HbT), oxy-hemoglobin (HbO) or deoxy-hemoglobin (HbR) in contrast to a functional MRI that can only measure HbR sensitive blood oxygen level dependent (BOLD) signals [1]. Currently, many functional NIRS studies have been conducted using topographic mapping based on the modified Beer-Lambert law (MBLL), and statistical analysis based on GLM for NIRS data has become popular. However, one of the main limitations of topographic map is its lack of depth information. For instance, monitoring occipital areas along a visual stimulus is often restricted in discriminating contralateral activation. On the other hand, retinotopic mapping with depth information, which is unattainable in topographic mapping, is feasible via tomographic approach using diffuse optical tomography (DOT) [2]. An inverse problem of DOT is, however, severely ill-posed due to the diffusive nature of light propagation. Therefore, a DOT suffers from low spatial resolution and depth sensitivity. To overcome these difficulties, various methods have been developed such as a spatio-temporal constraint using GLM [3], compressed sensing approach, and etc.

However, it is not clear how such advanced regularization scheme is related to the classical hypothesis driven approaches such as statistical parameter mapping (SPM) [4]. In this paper, we provide a novel compressed sensing approach for functional DOT problem that links advanced regularization schemes to SPM. More specifically, as the neural activation during task period is usually sparsely distributed and the temporal activation pattern is highly correlated with a predesigned paradigm, spatio-temporal sparsity of neural activation can be explicitly represented as a sparsity in statistical parameter map. To directly obtain t-map by exploiting its spatio-temporal sparsity, we employ a 2-thresholding algorithm that has been proven quite effective despite of its simplicity [5]. Interestingly, the resulting algorithm assumes a similar two step procedure to the conventional fDOT algorithms combined with SPM that first solves the minimum norm solution in spatial domain after which statistical parameter maps are obtained using GLM and p-value calculation. However, the main advantage of the proposed method is an iterative update of weighting component during the minimum norm solution, which is required to address given compressed sensing problem. We show that the reconstruction performance can be significantly improved by estimating the weighting component recursively, resulting in an iterative thresholding algorithm. Experimental results clearly show that the proposed iterative algorithm outperform the conventional algorithm and the accuracy of activation localization is quite competitive to fMRI.

2. BACKGROUND

2.1. Compressed Sensing using 2-thresholding

Compressive sensing (CS) theory [6] addresses accurate recovery of unknown sparse signals from underdetermined linear measurements. More specifically, let m and n be positive

This research was supported by the Korea Science and Engineering Foundation (KOSEF) grant funded by the Korea government (MEST) (No.2011-0000353).

integers such that $m < n$. Then, a noisy version of compressive sensing problem is given by

$$(P0): \quad \text{minimize} \quad \|\mathbf{x}\|_0 \quad \text{subject to} \quad \|\mathbf{y} - \mathbf{A}\mathbf{x}\| < \epsilon \tag{1}$$

where $\mathbf{y} \in \mathbb{R}^m$, $\mathbf{A} \in \mathbb{R}^{m \times n}$, $\mathbf{x} \in \mathbb{R}^n$, and $\|\mathbf{x}\|_0 = k$ denotes the k non-zero elements in the vector $\mathbf{x}$, and ϵ denotes the noise level. Among the algorithms to solve Eq. (1), we are interested in 2-thresholding method due to its computational simplicity and near optimality in low SNR cases [5]. In 2-thresholding, we select a set S with $|S| = k$ by taking correlation such that

$$\|\mathbf{a}_l^* \mathbf{y}\|_2 \geq \|\mathbf{a}_j^* \mathbf{y}\|_2, \text{ for all } l \in S,\ j \notin S.$$

How to select the unknown k in deterministic way is very difficult, however, it is switched to statistical inference in the proposed method as will be described later. In general, the performance of p-thresholding algorithm depends on the RIP of the dictionary, so high correlation between atoms significantly reduces the recovery performance. To overcome this difficulty, Schnass et al proposed a dictionary preconditioning [7] which applies a preconditioning weighting matrix $\mathbf{P} \in \mathbb{R}^{m \times m}$ to produce a new sensing matrix $\mathbf{PA}$ having a better RIP condition. If we use an optimal preconditioner $\mathbf{P} = \left(\mathbf{A}\mathbf{A}^T\right)^{-1/2}$ in the sense of minimizing Frobenius norm [7], then the correlation of the signal after the optimal preconditioning becomes

$$(\mathbf{PA})^T \mathbf{P}\mathbf{y} = \mathbf{A}^T(\mathbf{A}\mathbf{A}^T)^{-1}\mathbf{y} = \mathbf{A}^\dagger \mathbf{y}, \tag{2}$$

which corresponds to the minimum norm solution. Therefore, the optimized version of thresholding estimator for compressed sensing reconstruction can be implemented with minimum norm solution followed by thresholding to detect the support above a threshold value.

2.2. Forward Modeling

An optical flux variation at a detector position $\mathbf{r}_d$ from a source location at $\mathbf{r}_s$ can be approximated using the following Rytov approximation:

$$\Delta\phi(\mathbf{r}_d, \mathbf{r}_s; \lambda, t) \approx \int \frac{U_0(\mathbf{r}_d, \mathbf{r}; \lambda) U_0(\mathbf{r}, \mathbf{r}_s; \lambda)}{U_0(\mathbf{r}_d, \mathbf{r}_s; \lambda)} \Delta\mu_a(\mathbf{r}; \lambda, t) d\mathbf{r}, \tag{3}$$

where $\Delta\mu_a(\mathbf{r}; \lambda, t)$ is absorption variation at $\mathbf{r}$, λ denotes the illumination wavelength, and $U_0(\mathbf{r}, \mathbf{r}'; \lambda)$ is the optical flux at $\mathbf{r}$ generated from a source located at $\mathbf{r}'$. Here, we used two illumination wavelength, $\lambda_1 = 781mm$ and $\lambda_2 = 856mm$. Assuming that dynamically varying absorption contrast is mainly due to the oxygenation level changes in hemoglobin, we have

$$\Delta\mu_a(\mathbf{r}; \lambda, t) = a^\lambda_{HbO} \Delta c_{HbO}(\mathbf{r}; t) + a^\lambda_{HbR} \Delta c_{HbR}(\mathbf{r}; t), \tag{4}$$

where $a^\lambda_{HbO}[\mu M^{-1} mm^{-1}]$ and $a^\lambda_{HbR}[\mu M^{-1} mm^{-1}]$ are the extinction coefficients of HbO and HbR at wavelength of λ, and $\Delta c_{HbO}(\mathbf{r}; t)$ and $\Delta c_{HbR}(\mathbf{r}; t)$ are the concentration changes of HbO and HbR in a voxel $\mathbf{r}$ at time t, respectively. By collecting optical density variations for all time and pairs of detectors and sources, Eq. (3) can be represented in a matrix form as follows:

$$\begin{bmatrix} \mathbf{\Phi}^{\lambda_1} \\ \mathbf{\Phi}^{\lambda_2} \end{bmatrix} = \begin{bmatrix} a^{\lambda_1}_{HbO}\mathbf{G}^{\lambda_1} & a^{\lambda_1}_{HbR}\mathbf{G}^{\lambda_1} \\ a^{\lambda_2}_{HbO}\mathbf{G}^{\lambda_2} & a^{\lambda_2}_{HbR}\mathbf{G}^{\lambda_2} \end{bmatrix} \begin{bmatrix} \boldsymbol{\mathcal{H}}^T \\ \boldsymbol{\mathcal{R}}^T \end{bmatrix} + \begin{bmatrix} \mathbf{N}^{\lambda_1} \\ \mathbf{N}^{\lambda_2} \end{bmatrix}, \tag{5}$$

where $\mathbf{\Phi}^\lambda_{ij} = \Delta\phi(\mathbf{r}_{d_i}, \mathbf{r}_{s_i}; \lambda, t_j)$, $\mathbf{G}^\lambda_{ij} = \frac{U_0(\mathbf{r}_{d_i}, \mathbf{r}_j; \lambda) U_0(\mathbf{r}_j, \mathbf{r}_{s_i}; \lambda)}{U_0(\mathbf{r}_{d_i}, \mathbf{r}_{s_i}; \lambda)}$, $\boldsymbol{\mathcal{H}}_{ij} = \Delta c_{HbO}(\mathbf{r}_j; t_i)$, $\boldsymbol{\mathcal{R}}_{ij} = \Delta c_{HbR}(\mathbf{r}_j; t_i)$, and $\mathbf{N}^\lambda$ is a noise matrix at wavelength λ.

3. THEORY

3.1. Compressed Sensing Reconstruction of t-Map

Concentration changes of HbO and HbR in Eq. (5) can be represented in GLM as follows:

$$\boldsymbol{\mathcal{H}} = \mathbf{D}_{HbO} \cdot \boldsymbol{\mathcal{A}} + \mathbf{W}_H \quad \in \mathbb{R}^{J \times N}, \tag{6}$$

$$\boldsymbol{\mathcal{R}} = \mathbf{D}_{HbR} \cdot \boldsymbol{\mathcal{B}} + \mathbf{W}_R \quad \in \mathbb{R}^{J \times N}, \tag{7}$$

where $\mathbf{D}_{HbO}$ and $\mathbf{D}_{HbR}$ denote the design matrices for HbO and HbR, respectively; $\boldsymbol{\mathcal{A}} = [\boldsymbol{\alpha}_1, \cdots, \boldsymbol{\alpha}_N]$ and $\boldsymbol{\mathcal{B}} = [\boldsymbol{\beta}_1, \cdots, \boldsymbol{\beta}_N]$ denote the response matrices for HbO and HbR, respectively, where the n-th column indicates the corresponding GLM parameter vector at the n-th voxel, and J is the number of time points. Now, we are interested in finding a transform from GLM parameter to t-maps for the direct reconstruction of the statistical parameter maps. Under the assumption that $\mathbf{D} = \mathbf{D}_{HbO} = \mathbf{D}_{HbR} \in \mathbb{R}^{J \times M}$, we can calculate the minimum norm solution for the problem Eq. (5) using the GLM constraint and the property of $(\mathbf{B}^T \otimes \mathbf{A})\text{vec}(\mathbf{X}) = \text{vec}(\mathbf{AXB})$ and $(\mathbf{A} \otimes \mathbf{B})^\dagger = \mathbf{A}^\dagger \otimes \mathbf{B}^\dagger$:

$$\begin{bmatrix} \boldsymbol{\mathcal{T}}^T \\ \boldsymbol{\tau}^T \end{bmatrix} = \mathbf{V} \begin{bmatrix} \mathbf{\Phi}^{\lambda_1} \\ \mathbf{\Phi}^{\lambda_2} \end{bmatrix} \mathbf{D}^{\dagger T} \mathbf{C}^T, \tag{8}$$

where the first rows of $\boldsymbol{\mathcal{T}} \in \mathbb{R}^{M \times N}$ and $\boldsymbol{\tau} \in \mathbb{R}^{M \times N}$ are the t-statistics for the HbO and HbR of our interest, respectively; the inversion kernel $\mathbf{V}$ is

$$\mathbf{V} = \begin{bmatrix} a^{\lambda_1}_{HbO}\mathbf{G}^{\lambda_1}\mathbf{\Sigma}_{HbO} & a^{\lambda_1}_{HbR}\mathbf{G}^{\lambda_1}\mathbf{\Sigma}_{HbR} \\ a^{\lambda_2}_{HbO}\mathbf{G}^{\lambda_2}\mathbf{\Sigma}_{HbO} & a^{\lambda_2}_{HbR}\mathbf{G}^{\lambda_2}\mathbf{\Sigma}_{HbR} \end{bmatrix}^\dagger = \begin{bmatrix} \mathbf{V}^T_{HbO} \\ \mathbf{V}^T_{HbR} \end{bmatrix},$$

and $\mathbf{\Sigma}_{HbX} \in \mathbb{R}^{N \times N}$ are diagonal matrix whose (i,i)-th elements is $\sigma_{HbX,i}$, and $\mathbf{C}$ consists of a contrast vector to select a weighted combination of columns in the design matrix $\mathbf{D}$ and augmented any submatrix to make $\mathbf{C}$ invertible.

The second step of 2-thresholding base on compressed sensing reconstruction of t-map is thresholding, which is equivalent to the inference step in SPM using thresholding for a given p-value. In [8], we employed the expected Euler Characteristics (EC) approach in terms of Lipschitz-Killing curvatures for inhomogeneous t-statistics and demonstrated its equivalence to the tube formula. Hence, we use this for $3D$ case as well.

3.2. Iterative Improvement

There are two important issues in actual implementation of the proposed compressed sensing algorithm. First, we should be aware that the variance matrices $\mathbf{\Sigma}_{HbO}$ and $\mathbf{\Sigma}_{HbR}$ are dependent on the solution of the inverse solution $\boldsymbol{\mathcal{H}}$ and $\boldsymbol{\mathcal{R}}$ as follows [4]:

$$\hat{\sigma}^2_{HbO,n} = \frac{\mathbf{h}_n^T \mathbf{P}_{\mathbf{D}}^{\perp} \mathbf{h}_n}{\mathrm{trace}(\mathbf{P}_{\mathbf{D}}^{\perp} \mathbf{\Lambda})}, \; n = 1, \cdots, N, \tag{9}$$

where $\mathbf{P}_{\mathbf{D}}^{\perp} = \mathbf{I} - \mathbf{D}\mathbf{D}^{\dagger}$ and $\mathbf{h}_n$ is the n-th column of $\boldsymbol{\mathcal{H}}$, $\mathbf{\Lambda}$ denotes the temporal correlation matrix calculated by 'precoloring' approach, and $\hat{\sigma}^2_{HbR,n}$ is calculated similarly. Since these are the unknown values we need to reconstruct, the problem is highly nonlinear. In order to overcome the technical difficulty, we propose an iterative update. More specifically, we first solve the minimum norm solution assuming that the variance matrix is identity, i,e, $\mathbf{\Sigma}_{HbO} = \mathbf{\Sigma}_{HbR} = \mathbf{I}_N$. Then, using the reconstructed inverse solution $\boldsymbol{\mathcal{H}}$ and $\boldsymbol{\mathcal{R}}$, we update the variance matrix and solve the minimum norm solution again with the updated variance matrices. This procedure can be repeated until convergence. Note that the first step of this iterative refinement is equivalent to the conventional fDOT followed by SPM analysis. We will show that this iterative refinement is very important and significantly improve the reconstruction performance of t-map.

Another important observation is that

$$\hat{\sigma}^2_{HbX,n,new} = \mathbf{v}^T_{HbX,n} \mathbf{\Sigma} \mathbf{v}_{HbX,n} \, \hat{\sigma}^2_{HbX,n,old}, \tag{10}$$

where

$$\mathbf{\Sigma} = \frac{1}{\mathrm{trace}\left(\mathbf{P}_{\mathbf{D}}^{\perp} \Lambda\right)} \begin{bmatrix} \mathbf{\Phi}^{\lambda_1} \\ \mathbf{\Phi}^{\lambda_2} \end{bmatrix} \mathbf{P}_{\mathbf{D}}^{\perp} \begin{bmatrix} \mathbf{\Phi}^{\lambda_1 T} & \mathbf{\Phi}^{\lambda_2 T} \end{bmatrix} \tag{11}$$

where $\mathbf{v}_{HbX,n}$ denotes the n-th column of $\mathbf{V}_{HbO}$ (or $\mathbf{V}_{HbR}$), respectively. Since $\mathbf{\Sigma}$ is common regardless of iteration, we calculate this matrix once and just change the inverse Kernel $\mathbf{V}$ at each iteration to update the variance component. Therefore, the compressed sensing reconstruction of t-map in DOT problem can be implemented using the following approach;

1. Initialization : $\mathbf{\Sigma}_{HbO,old} = \mathbf{\Sigma}_{HbR,old} = \mathbf{I}_N$
2. Update $\mathbf{V}$ with $\mathbf{\Sigma}_{HbX,old}$ and calculate $\mathbf{\Sigma}_{HbX,new}$ using Eq. (10).
3. If $\mathbf{\Sigma}_{HbX,new}$ is converged then go to next step, otherwise set $\mathbf{\Sigma}_{HbX,old} \leftarrow \mathbf{\Sigma}_{HbX,new}$ and go to previous step.
4. Calculate intermediate GLM parameter matrices for raw data measured at wavelengths λ_1 and λ_2 using the ordinary least squares:
$$\begin{bmatrix} \mathbf{B}^{\lambda_1 T} \\ \mathbf{B}^{\lambda_2 T} \end{bmatrix} = \begin{bmatrix} \mathbf{\Phi}^{\lambda_1} \\ \mathbf{\Phi}^{\lambda_2} \end{bmatrix} \left(\mathbf{D}^{\dagger}\right)^T$$
5. Find the GLM parameter for HbO and HbR from the GLM parameters for raw data as the minimum norm solution:
$$\begin{bmatrix} \boldsymbol{\mathcal{A}}^T \\ \boldsymbol{\mathcal{B}}^T \end{bmatrix} = \begin{bmatrix} \mathbf{\Sigma}_{HbO,old} & \mathbf{0} \\ \mathbf{0} & \mathbf{\Sigma}_{HbR,old} \end{bmatrix} \mathbf{V} \begin{bmatrix} \mathbf{B}^{\lambda_1 T} \\ \mathbf{B}^{\lambda_2 T} \end{bmatrix}$$
6. Apply the contrast matrix to obtain the t-map
$$\boldsymbol{\mathcal{T}} = \mathbf{C}\boldsymbol{\mathcal{A}}\mathbf{\Sigma}^{-1}_{HbO,new} \quad , \quad \boldsymbol{\tau} = \mathbf{C}\boldsymbol{\mathcal{B}}\mathbf{\Sigma}^{-1}_{HbR,new}$$
7. Apply thresholding of the calculated t-maps.

4. RESULTS

4.1. Simulation Results

We performed a simulation study for localization of the activation area to confirm the performance improvement with the iteration. The source and detector geometry is illustrated in Fig. 1(a), and is identical with the real NIRS system (Oxymon MK III, Artinis, Netherlands). We assume that the activation area has a sphere shape with radius of $2mm$ and is placed in the cortical layer as indicated in Fig. 1(a) with a big arrow. Temporal concentration changes for oxy- and deoxy-hemoglobin in the activation area is illustrated in Fig. 1(b). Fig. 1(c) shows the centers of various synthetic activation ($19.8 \sim 45.3mm$) during our experiments. We used 17 channels and added Gaussian noise with SNR of $10dB$ at the measurements followed by hemodynamic response function (HRF) smoothing.

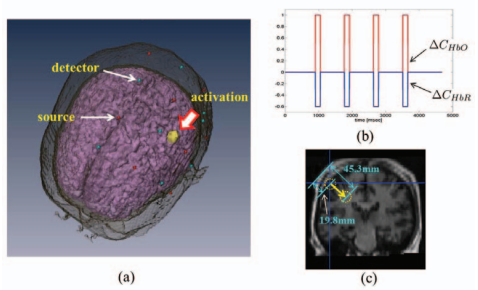


Fig. 1. (a) Simulation setup to validate the proposed method, (b) temporal change of HbO(red) and HbR(blue), and (c) trajectory of the center of the activation area.

Figs. 2(a)(b) illustrate the minimum displacement error between the ground truth activation and the position of the peak value of the estimated t-statistic map of HbO and HbR, with respect to various number of iterations. The results are averaged after 500 runs. As shown in Fig. 2(a), the accuracy improves as the number of iteration increases. Furthermore, the improvement with iteration is bigger as the activation area is nearer to the surface. At the area of deeper than $37mm$, the displacement error is nearly same regardless of the number of iteration. The tendency of the result of HbR is similar with HbO as shown in Fig. 2(b).

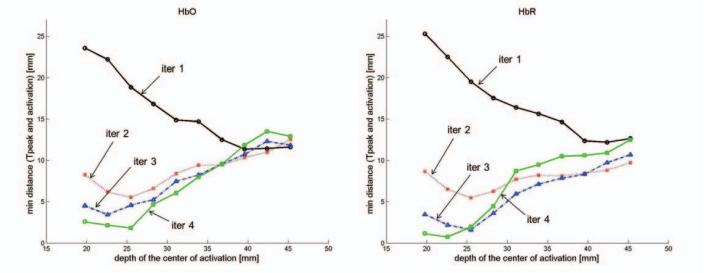


Fig. 2. Minimum distance $[mm]$ between the ground truth activation and the position of the peak value of the t-map.

4.2. *In vivo* Experimental Results

To demonstrate the performance of the proposed method in *in vivo* experiments, we used data from right finger tapping experiment for three subjects. The activation map of fDOT using the proposed method is compared to the golden standard fMRI activation map. The t-maps from fDOT and fMRI are thresholded with a corrected p-value of 0.05 and then their intersection with the region of interest are considered. The source and detector geometry is identical to Fig. 1(a) and we also used 17 channels from the NIRS system.

We visualized the activation map of subject 3(HbR) for number of iteration 1(Figs. 3(a)(b)) and 2(Figs. 3(c)(d)). Figs. 3(a)(c) are 3D rendering of the activation map (yellow:fMRI, cyan:fDOT, red:common area for fMRI and fDOT). Figs. 3(b)(d) are 3 views with coronal, midsagittal, and horizontal section (the cross hair indicates the position of the peak value of t-statistic map). Note that the wide-spreading activation area of fDOT with iteration 1 is greatly reduced for iteration 2 as shown in Fig. 3(a) and Fig. 3(c) especially in the region indicated with big arrow.

Next, we calculated center of mass (COM) for the activation area and summarized the distance of COM to each other (fDOT versus fMRI) or to primary motor cortex (PMC) and somatosensory cortex (SSC) for each imaging modality in Table 1. In the majority of cases, we can see the advantage of using more iterations for fDOT method. Note that the distance of COM between fMRI and fDOT(HbR) has the accuracy up to $11.63 \pm 1.92mm$ by using 3 iterations.

Table 1. Distance [mm] of COM to each other (fDOT versus fMRI) or to PMC and SSC.

	iter	fDOT (HbO)			fDOT (HbR)			fMRI	
		COM	PMC	SSC	COM	PMC	SSC	PMC	SSC
subj 1	1	34.45	10.98	18.48	10.46	7.29	3.06	7.56	3.59
	2	26.43	12.13	14.76	8.52	6.35	3.12		
	3	22.89	14.05	15.08	10.48	8.01	6.04		
subj 2	1	25.51	16.44	21.53	25.96	13.15	15.82	1.87	1.15
	2	28.86	18.39	23.06	23.75	14.05	14.94		
	3	31.46	17.63	21.67	13.03	5.21	4.46		
subj 3	1	35.21	4.34	13.05	20.86	12.53	14.81	2.33	5.13
	2	34.46	4.28	11.76	13.16	4.97	7.91		
	3	36.19	2.45	11.58	13.47	5.73	8.54		
Group	1	19.24	11.62	13	11.89	7.25	9.99	7.61	4.96
	2	11.16	8.28	10.15	8.69	6.64	7.82		
	3	9.16	7.12	8.55	9.55	7.18	8.61		

5. CONCLUSION

In this paper we proposed a compressed sensing reconstruction using 2-thresholding algorithm for functional diffuse optical tomography. Interestingly, the first step of the proposed iterative method is identical to the conventional minimum norm solution approach. The main advantage of our algorithm is that the weighting component in the inversion kernel can be updated to improve the accuracy of the reconstruction. Finally, we showed that the thresholding step of 2-thresholding algorithm is equivalent to the inference step in SPM framework. Simulation and experimental results demonstrated that the proposed method improves the reconstruction accuracy by iteration and is competitive with that of fMRI.

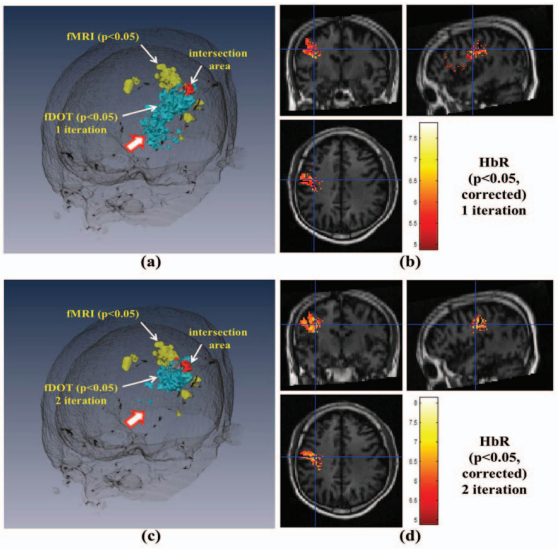


Fig. 3. Activation map ($p < 0.05$, corrected) for fMRI and fDOT(HbR) with different number of iteration.

6. REFERENCES

[1] A. Villringer and B. Chance, "Non-invasive optical spectroscopy and imaging of human brain function," *Trends Neurosci.*, vol. 20, pp. 435–442, 1997.

[2] B. W. Zeff, B. R. White, H. Dehghani, B. L. Schlaggar, and J. P. Culver, "Retinotopic mapping of adult human visual cortex with high-density diffuse optical tomography," *Proc. Nati. Acad. Sci. USA*, vol. 104, no. 29, pp. 12169–12174, 2007.

[3] Y. Zhang, D. H. Brooks, and D. A. Boas, "A haemodynamic response function model in spatio-temporal diffuse optical tomography," *Phys. Med. Biol.*, vol. 50, pp. 4625–4644, 2005.

[4] K. J. Friston, J. Ashburner, S. Kiebel, T. Nichols, and W. Penny, Eds., *Statistical parametric mapping: The analysis of functional brain images*, Academic Press, Sandiego, CA, USA, 2006.

[5] A.K. Fletcher, S. Rangan, and V.K. Goyal, "Necessary and sufficient conditions for sparsity pattern recovery," *IEEE Trans. on Information Theory*, vol. 55, no. 12, pp. 5758–5772, 2009.

[6] D. L. Donoho, "Compressed sensing," *IEEE Trans. on Information Theory*, vol. 52, no. 4, pp. 1289–1306, April 2006.

[7] K. Schnass and P. Vandergheynst, "Dictionary preconditioning for greedy algorithms," *IEEE Trans. on Signal Processing*, vol. 56, pp. 1994–2002, 2008.

[8] H. Li, S. Tak, and J. C. Ye, "Lipschitz killing curvature based expected euler characteristics for p-value correction in fNIRS," *to appear in J. Neurosci. Meth.*, 2011.